ELSEVIER

Journal of Nuclear Materials 265 (1999) 60–68

journal of nuclear materials

Determination of the β/β + γ eutectoid transition temperature in ZrO_{2-x} at variable heating/cooling rates

P.J. Hayward *, I.M. George

Atomic Energy of Canada Limited, Whiteshell Laboratories, Pinawa, Manitoba R0E 1L0, Canada

Received 10 June 1998; accepted 23 September 1998

Abstract

The temperature at which ZrO_{2-x} undergoes a eutectoid transition from tetragonal (β) to tetragonal + cubic (β + γ) structure has been measured using oxidized Zircaloy-4 specimens, a pyrometer-based differential thermal analysis technique, and heating/cooling rates in the range 19–569 K/min. The transition was found to be completely reversible, showed no hysteresis and was essentially independent of heating/cooling. The overall temperature uncertainty was obtained by combining calibration, pyrometer reproducibility, thermal lag and systematic errors. A transition temperature of 1786 ± 12 K is recommended for use in Zircaloy/steam oxidation-rate correlations employed in reactor safety codes.

1. Introduction

During the high-temperature transient phase of a severe-fuel-damage (SFD) reactor accident, failure or blockage of the cooling circuit may form a steam or steam/hydrogen atmosphere that, together with decay heat from the bundle, initiates oxidation of the outer Zircaloy-4 cladding surfaces. The reaction is highly exothermic and may be summarized as

$$Zr + H_2O \rightarrow ZrO_2 + 2H_2 + \Delta H, \quad (1)$$

where ΔH, which represents the heat of formation of one mole of ZrO_2 from its elements minus the heat required to dissociate two moles of steam, is equal to ~586 kJ/mol at 1600 K. At temperatures above ~1473 K, this reaction controls the amount of hydrogen formed during the transient and is also a significant factor in determining the peak temperatures experienced by the fuel bundles.

One commonly used method for modelling the Zircaloy-steam reaction during a transient, such as that employed in the CATHENA code [1], is based on considering the reaction as a succession of short isothermal periods, using parabolic rate constants derived from isothermal heating experiments [2–7]. With the exception of the early Baker–Just data [7], the high-temperature isothermal oxidation data [2–4] show a step increase in oxidation rate by a factor of 2–3 at a temperature within the range 1783–1850 K, as shown in Fig. 1. The increase has been attributed to the onset of formation of cubic (γ) zirconia within the oxide layer, giving an enhanced rate of oxygen diffusion through the oxide to the underlying metal. This sudden increase in oxidation rate is also incorporated in transient-oxidation models based on isothermal data.

To examine the validity of this modelling approach, it is necessary to consider the thermodynamic and kinetic aspects of zirconia phase formation. Fig. 2 shows the relevant part of the Zr-O phase diagram, based on data from [8] and references therein; this data has also been used in subsequent phase diagram compilations [9,10]. The stable forms of stoichiometric ZrO_2 are (i) the monoclinic (α) phase up to ~1478 K, (ii) the tetragonal (β) phase within the temperature range ~1478–~2650 K, and (iii) the cubic (γ) phase up to the melting temperature of ~2980 K.

The phase relations of the hypostoichiometric oxides are rather more complex, however, and depend on the O/Zr ratio. Although there is some uncertainty in the exact location of the phase boundaries in Fig. 2, the

* Corresponding author. Tel.: +1-204 753 8338; e-mail: haywardp@mb.sympatico.ca

0022-3115/99/$ – see front matter
PII: S0022-3115(98)00620-5

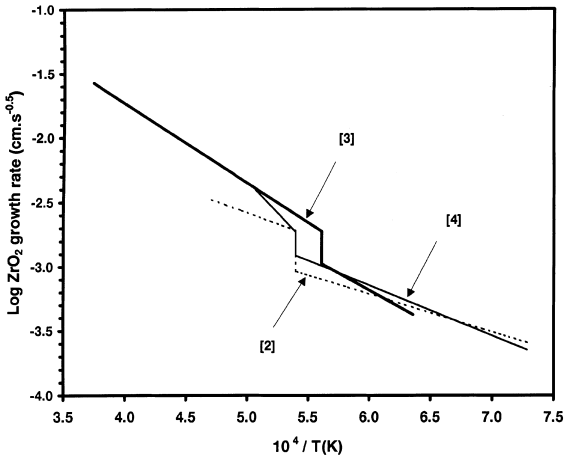

Fig. 1. Parabolic rate constants for oxide layer growth during isothermal steam oxidation of Zircaloy-4; data from Refs. [2–4].

diagram may be interpreted as follows. Slow heating of an equilibrium mixture of co-existing [α-Zr(O) + β-$ZrO_{1.98}$] to just beyond the eutectoid-reaction-isotherm temperature (subsequently referred to as T_e) at ~1773 K will cause precipitation of the γ-oxide to commence.

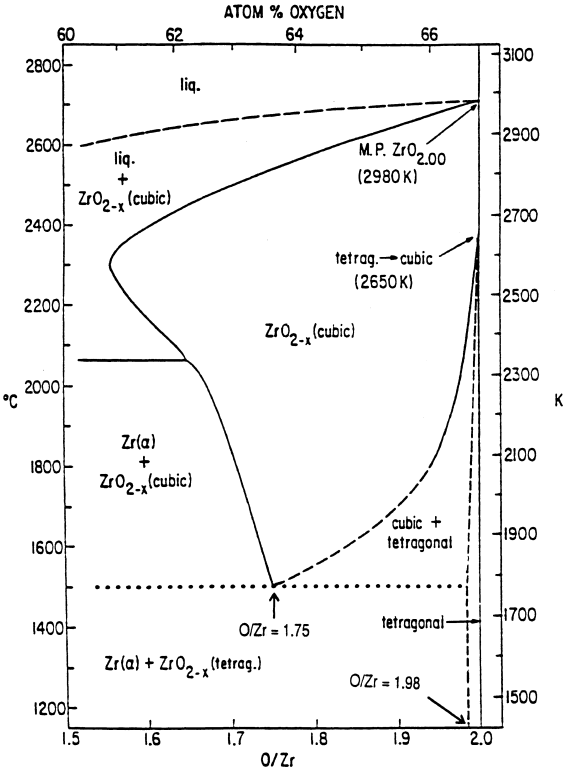

Fig. 2. The ZrO_{2-x} region of the Zr-O phase diagram, after Ref. [8].

Depending on the O/Zr ratio, the eutectoid reactions may be summarised by the following generalized equations:

For O/Zr = 1.75–1.98:

$$\alpha\text{-Zr(O)} + \beta\text{-}ZrO_{1.98} \rightarrow \gamma\text{-}ZrO_{1.75} + \beta\text{-}ZrO_{1.98}, \quad (2)$$

For O/Zr = 0.45–1.75:

$$\alpha\text{-Zr(O)} + \beta\text{-}ZrO_{1.98} \rightarrow \gamma\text{-}ZrO_{1.75} + \alpha\text{-Zr(O)}. \quad (3)$$

The relative proportions of the reaction products are determined by the initial O/Zr ratio in accordance with the lever rule. In both cases, cooling below T_e will eventually cause the reaction to be reversed.

These reactions require oxygen transport between the various phases. Thus, the rate at which equilibrium is achieved will depend on the separation between phase regions and on the oxygen diffusion coefficients within each phase. The chemical diffusion of oxygen in hypostoichiometric ZrO_{2-x} phases is known to occur rapidly by migration across the relatively high concentration of O vacancies. In practice, however, high-temperature steam oxidation of fuel cladding occurs too rapidly for equilibration to occur. Typically, an oxygen concentration gradient will exist across steam-oxidized cladding, giving rise to a sequence of phases from the outer to the inner surface, as follows:

Above T_e: near-stoichiometric β-ZrO_2/hypostoichiometric γ-ZrO_{2-x}/α-Zr(O)/β-Zr.

Below T_e: near-stoichiometric β-ZrO_2/α-Zr(O)/β-Zr.

These sequences are easily recognised in sectioned specimens of steam-oxidized Zircaloy. The duplex oxide layer formed above T_e can be distinguished by the characteristic microstructures produced on cooling through the γ/β and/or the β/α transition temperatures (see, for example, Fig. 8 in Ref. [3], also published as Fig. 7 in Ref. [11]).

Thus, the validity of using isothermal oxidation data to model cladding oxidation during a transient depends on a number of uncertain factors. If the transient heating rate greatly exceeds the rate at which the equilibrium zirconia phases can form, the relative thicknesses of the tetragonal and cubic layers will differ from those produced under isothermal conditions. In this case, the effective O-diffusion rate through the duplex layer (and, hence, the oxidation rate) could show a smooth increase at T_e rather than the step change that is used in existing models.

A further uncertainty lies in the value for T_e used for modelling. Current estimates are based either on Zr-O phase-equilibrium studies [8–10] or on isothermal oxidation data [2–4], and vary by as much as 70 K. This variation can lead to widely ranging predictions for the

volume of hydrogen produced and the peak temperature attained. As a consequence, many cladding oxidation models use an assumed value for T_e, such as the value of 1800 K value employed in the FROM.SFD/Mk2 code [12].

One of the objectives of the experimental work described below was to reduce the uncertainty in T_e by performing new measurements. A further objective was to assess whether the measured T_e values were significantly dependent on the heating/cooling rate during thermal cycling across the eutectoid reaction isotherm. This latter consideration could have important implications for modelling the Zircaloy steam reaction under different accident conditions, where the predicted heating rates may be very different. For example, in a CANDU [1] flow-blockage scenario, where the reactor remains at full power, fuel temperatures may increase at several hundred K/s. During the early stages of a large-break loss-of-coolant accident (LOCA), the power pulse from stored energy within the fuel can produce heating rates of, typically, 30–40 K/s. In the later stages of a LOCA with concomitant loss of emergency coolant injection, the predicted heating rates are $\leqslant 5$ K/s [13].

An obvious method of measuring T_e would be to perform conventional (thermocouple-based) differential thermal analysis (DTA) on equilibrated samples of α-Zr(O) + ZrO_{2-x}. Typically, however, this technique is limited to heating/cooling rates of $\leqslant 1$ K/s, which are too low to simulate most reactor accident scenarios. For this reason, the T_e measurements were performed with the widest practical range of heating and cooling rates, using a pyrometer-based DTA (PDTA) technique that allowed heating/cooling rates in the range 0.3–~9 K/s to be used.

2. Experimental

2.1. Specimen preparation

The oxidized Zircaloy specimens were prepared from a series of 6.35 mm diameter, 1.5 mm thick disks cut from Teledyne Wah Chang Zircaloy-4 rod. These disks were placed on yttria wafers and individually oxidized at 1273 K under flowing Ar/25%O_2 in a thermobalance, terminating the oxidation when approximately 67% of the Zircaloy had been converted to a thick oxide skin around an oxygenated alloy core. Final annealing was performed on a graphite substrate within a tungsten resistance furnace immediately prior to the PDTA runs by holding each specimen at 1723 K for 60 min under ultra-high-purity (UHP) argon before commencing the run.

The intention of this final annealing stage was to allow the oxide to partially re-dissolve in the alloy core, thereby moving the surface oxide composition to a point on the lower β-ZrO_{2-x} phase boundary. Fig. 3 is an optical micrograph of a surface region from a control specimen that was oxidized, annealed at 1723 K for 60 min, and then cooled. The micrograph shows numerous regions of α-Zr(O) within the oxide matrix. Some of these alloy regions were undoubtedly produced by disproportionation during cooling through the β/α transition at ~1478 K, according to the generalized reaction

$$\beta\text{-}ZrO_{1.98} \rightarrow \alpha\text{-}ZrO_2 + \alpha\text{-}Zr(O). \quad (4)$$

The abundance of alloy regions in Fig. 3 is far too great, however, to have been caused solely by this reaction, which typically produces only 1–2 vol.% α-Zr(O) [2]. Thus, the majority must have been formed during the annealing process as a result of O diffusion to the central region of the specimen.

2.2. PDTA technique

The PDTA measurements were performed in a Centorr tungsten resistance furnace, which was coupled to a programmable controller via a Type C thermocouple. The specimen under investigation was placed on top of an 8-mm-side cube of high-density graphite that, in turn, rested on an upturned thin-walled alumina crucible to provide thermal insulation from the furnace stage.

A dual wavelength pyrometer was focused on the upper specimen surface through a silica-glass window in the furnace roof. A similar dual wavelength pyrometer

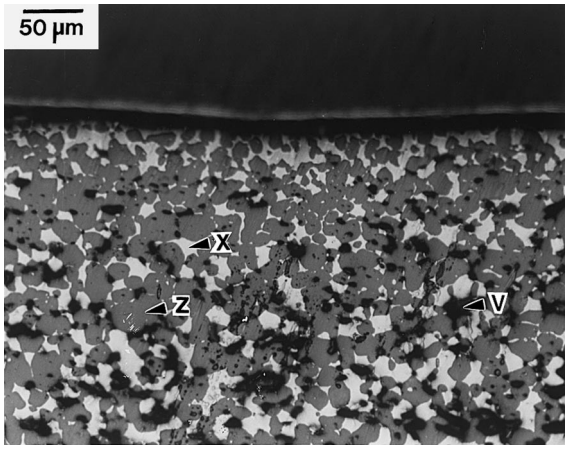

Fig. 3. Optical micrograph of the sectioned surface of a Zircaloy specimen after oxidation and annealing: X = α-Zr(O); Z = prior-β zirconia; V = void.

[1] Registered trademark of Atomic Energy of Canada Limited.

was focused on the graphite surface through a second window in the furnace sidewall, with the emittance-ratio slope (*E*-slope) setting appropriate for a black-body. A computer-based data acquisition system was used to record the output of both pyrometers. The assembly is shown schematically in Fig. 4.

After evacuating and backfilling with UHP argon, the furnace was heated to 1723 K and held for 60 min at this temperature for final annealing of the specimen (see above). The temperature was then raised to 1773 K (i.e., just below the anticipated transition temperature), and held for 5 min to allow temperature equilibration. After this time, an empirical correction for specimen emissivity was made, assuming that the specimen and black-body were at the same temperature, by adjusting the *E*-slope potentiometer of the specimen pyrometer to bring the recorded temperature into agreement with the temperature measured by the black-body pyrometer.

The furnace was cooled to 1723 K and then programmed to cycle three times over the temperature range 1723–1923 K at a fixed heating/cooling rate. During each ramp, the specimen and black-body temperatures were simultaneously recorded at an appropriate rate to give adequate data resolution. The target heating/cooling rates were 20, 30, 40, 100, 200, 400, 600 and 800 K/min, with data acquisition rates (Hz) of 1, 1, 1, 2, 3, 4, 6 and 8, respectively. The heating/cooling rates achieved were somewhat lower than the target values, however, because of thermal inertia in the system.

Fresh specimens were used for each of the PDTA runs with target heating/cooling rates of 20, 30, 40 or 100 K/min. The results for each thermal cycle were almost identical, and did not vary significantly with heating/cooling rate, implying that any reaction occurring in the surface layer was completely reversible. Hence, a new specimen was used for the PDTA runs with a target heating/cooling rate of 200 K/min, and further runs with target rates of 400, 600 and 800 K/min were performed immediately afterwards using the same specimen.

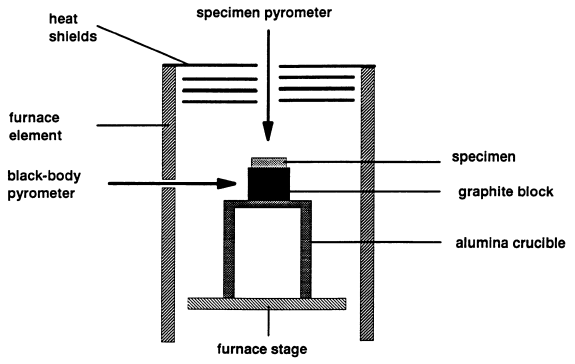

Fig. 4. Schematic diagram of PDTA assembly.

The recorded time/temperature data were subsequently analysed, smoothed (see Section 3) and plotted as traces of the temperature difference between the specimen and the black-body cavity (ΔT_{s-bb}) versus the black-body cavity temperature (T_{bb}).

2.3. Calibration

An initial estimate was made of any thermal lag between the top and side faces of the graphite cube during heating as a consequence of their being directly facing, or at right angles to, the tungsten heating element. With no specimen present, the graphite face temperature was recorded during heating at 20 K/min over the temperature range 1723–1873 K. The top-face temperature lagged behind the side-face temperature by $\leqslant 1$ K, with the lag remaining constant throughout each run.

The system was calibrated by measuring the melting point of a 99.999% pure Fe specimen, contained in an yttria crucible, while cycling the temperature at 20 K/min for three times within the range 1723–1923 K. The resulting ΔT_{s-bb} versus T_{bb} plots for Fe gave peak onset temperatures of 1810 ± 1 K, in excellent agreement with the literature value of 1811 K [7].

2.4. Optical and SEM/EDX analyses of post-test specimens

To confirm that the transition temperature measurements had been performed with co-existing [ZrO_{2-x} + α-Zr(O)], selected post-test specimens were sectioned, polished and examined by reflected light and scanning electron microscopy (SEM). Fig. 5(a) shows a low magnification backscattered electron (BSE) micrograph of a specimen after numerous thermal cycles at nominal ramp rates of 200–800 K/min. The lower oxide surface had lifted away from the main part of the specimen as a result of the large volume contraction that occurs during final cooling through the β/α transition at ~1478 K. Quantitative energy-dispersive X-ray (EDX) analysis for Zr and O confirmed that the outer regions of this specimen contained ZrO_{2-x} and α-Zr(O), with a core of α-Zr(O). The void in the centre of the core was produced by oxidation of β-Zr to the denser α-Zr(O) phase.

Fig. 5(b) is an optical micrograph of a sectioned surface region from another specimen after thermal cycling. Comparison with Fig. 3 shows that a significant fraction of the α-Zr(O) phase had migrated to the specimen surface, leaving voids in the sub-surface oxide material. This migration may have been encouraged by repeated precipitation and re-solution of α-Zr(O) during cooling and heating through T_e, respectively, as a result of the differing O/Zr ratios in γ- and β- zirconia (see Eq. (2)).

Fig. 5(c) is a BSE image of the oxide interface with the alloy material near the central part of a

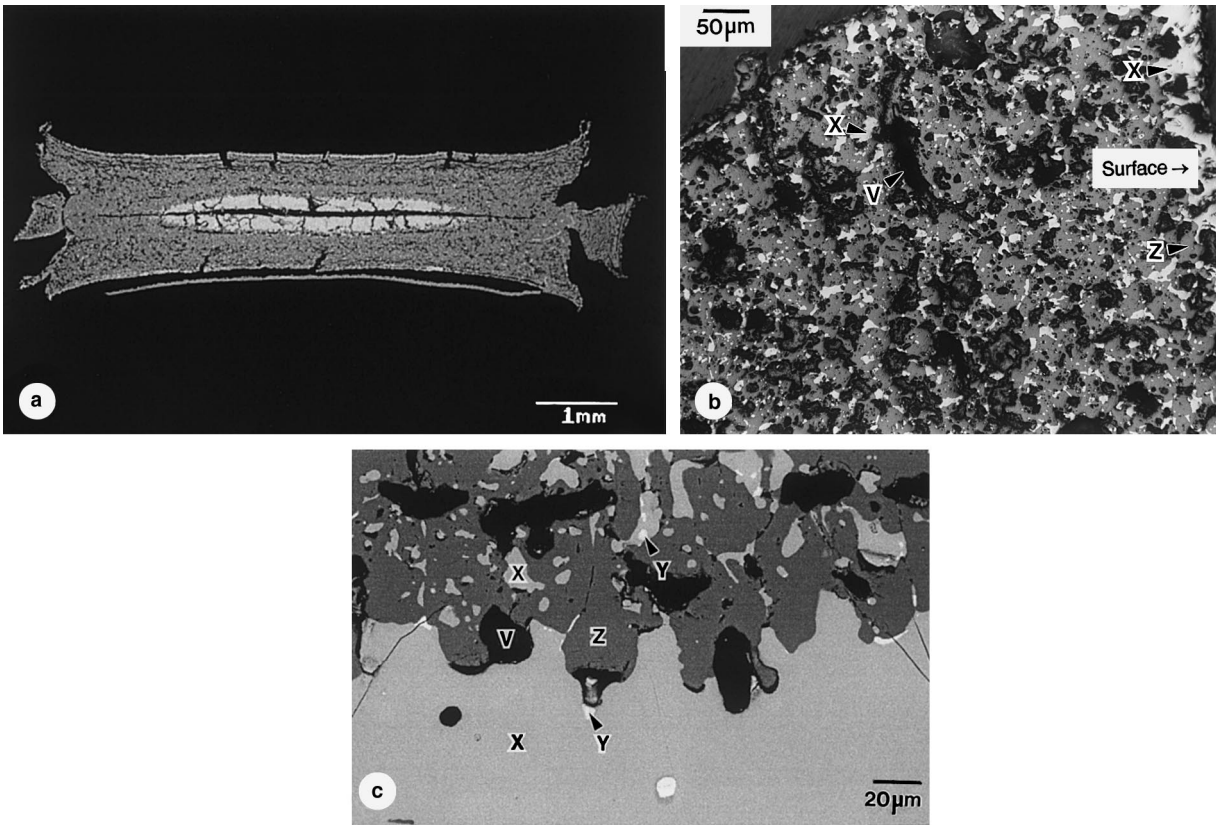

Fig. 5. (a) BSE micrograph of test specimen after repeated thermal cycling at 200–800 K/min. (b) Optical micrograph of specimen surface after thermal cycling: X = α-Zr(O); Z = prior-γ zirconia; V = void. (c) BSE image of oxide/alloy interface after thermal cycling: X = α-Zr(O); Z = prior-γ zirconia; Y = Zr/Sn alloy; V = Void.

thermally-cycled specimen. These ZrO_{2-x} regions also contained precipitates of α-Zr(O). In addition, minor quantities of dispersed Zr/Sn or Zr/Fe/Cr alloy phases were observed. The latter were presumably formed by exclusion of Sn, Fe and Cr from the oxide structure during Zircaloy oxidation.

3. Results

The plots of raw ΔT_{s-bb} versus T_{bb} data displayed somewhat noisy backgrounds because of power oscillations created by the furnace controller in attempting to follow the program. Hence, a moving-average smoothing procedure was used on the raw data to allow clear resolution of the peaks without changing the peak onset temperatures. Fig. 6 shows plots of original and smoothed data from a 566 K/min heating run to illustrate the effect of smoothing.

The smoothed plots all showed an endothermic PDTA peak during heating and an exothermic peak during cooling. This feature would be expected in the case of a first order transition, in which a discontinuous change in the Gibbs free energy function occurs at the transition temperature [14]. Typical examples of first order transitions include melting/freezing or crystallographic transitions in which there is no change in composition, such as occurred during melting of the Fe specimen used to calibrate the system. The origin of the peaks in the PDTA results for the oxide disks is more complex, however, and is discussed in Section 4.1.

In general, the temperature at which a specimen undergoes a transition is given by the peak onset temperature, i.e., the temperature at which the PDTA trace begins to depart from the baseline. In practice, however, the temperature of the specimen interior will always lag behind that of the surface during heating or cooling, causing the peak to widen and to return to the baseline only after the entire specimen has undergone the transition. It follows that the temperature at the peak maximum and also the peak width, are functions of specimen size and thermal conductivity, and have no fundamental meaning. As the heating or cooling rate increases, the increased thermal lag causes the peak to

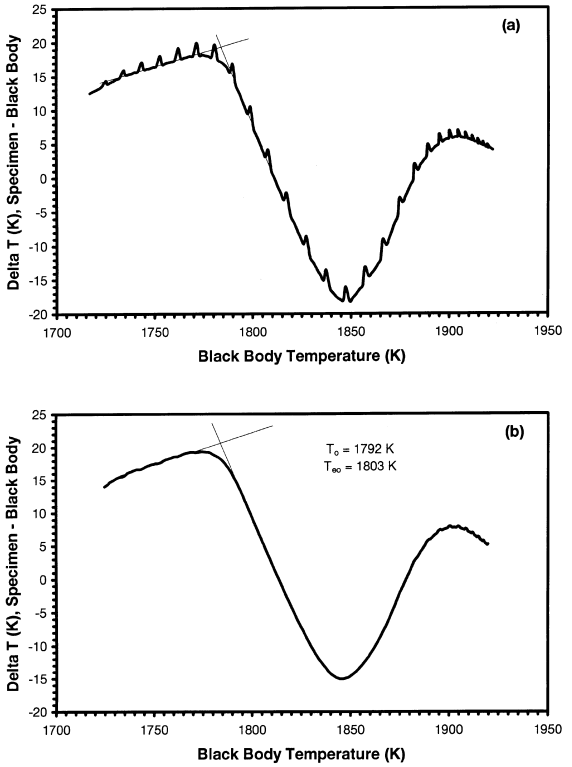

Fig. 6. PDTA traces, 566 K/min heating, 2nd cycle: (a) not smoothed; (b) smoothed.

broaden and the peak amplitude to decrease. However, the peak onset temperature should, in theory, remain unchanged.

There are two possible methods for deriving the transition temperature from each smoothed ΔT_{s-bb} versus T_{bb} data set. It is common practice in conventional DTA analysis to define a transition temperature from the intersection of extrapolated lines representing the baseline and the appropriate side of the peak. This is referred to as the *extrapolated onset temperature* (T_{eo}) for the endothermic peak observed on heating or the exothermic peak observed on cooling. This method of determining the peak onset temperature is most appropriate for DTA runs performed at relatively low ($\leqslant 20$ K/min) heating or cooling rates, when the thermal lag across the specimen is insignificant In the PDTA traces, T_{eo} is given by $\Delta T_{s-bb} + T_{bb}$ at the point of departure from the trace baseline.

Because PDTA is a dynamic procedure, the surface of a specimen will always reach the transition temperature before the specimen interior. At faster heating/cooling rates ($\geqslant 20$ K/min), the time difference between the transition occurring at the specimen surface and in the interior material will become increasingly significant. Hence, the transition temperature is probably more accurately defined by the temperature at which the ΔT_{s-bb} versus T_{bb} trace begins to depart from the baseline, i.e., when the surface material, whose temperature is being measured by one of the pyrometers, undergoes its transition. This temperature is subsequently referred to as the *onset temperature* (T_o), and is given by $\Delta T_{s-bb} + T_{bb}$ at the point on the trace corresponding to the peak onset.

The general shape of the PDTA traces is illustrated by Figs. 7 and 8, which show representative heating and cooling traces from one of the three cycles at 37 K/min and at 176–179 K/min, respectively. In general, the traces for each cycle at a particular heating or cooling rate were almost identical, indicating that the transition is completely reversible. The construction lines used to derive T_o and T_{eo} values are also shown. These lines were fitted to the curves by eye, so that there is a degree of subjectivity in assessing the point of departure of each trace from the baseline; the resulting errors in T_o and T_{eo} values are estimated to be $\sim\pm 2$ K. Table 1 lists the derived T_o and T_{eo} values as a function of the heating/cooling rate. We recommend that the T_o values be taken as representing the transition temperatures.

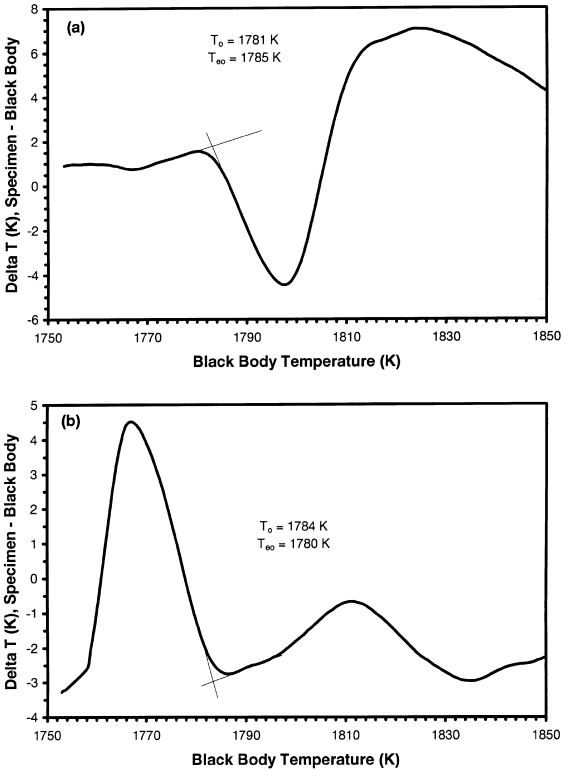

Fig. 7. Smoothed PDTA traces for 37 K/min runs, 1st Cycle: (a) heating; (b) cooling.

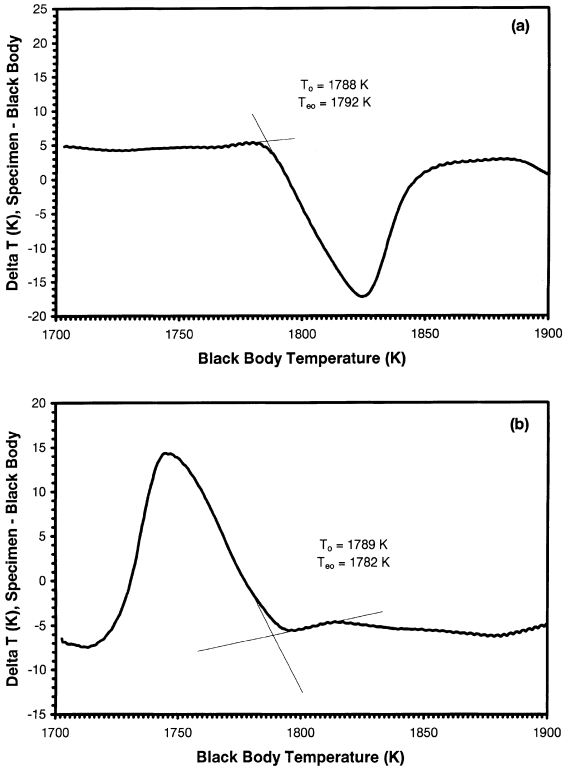

Fig. 8. Smoothed PDTA traces, 2nd cycle: (a) 176 K/min heating; (b) 179 K/min cooling.

4. Discussion

4.1. Transition mechanism

As noted above, the transition phenomenon indicated by the PDTA data appears to be completely reversible, shows no hysteresis, and is essentially insensitive to the heating/cooling rate. However, interpretation of the results in terms of the transition mechanism is complicated by the fact that the specimens were macroscopically inhomogeneous, ranging from a two-phase [α-Zr(O) + ZrO_{2-x}] mixture in the outer regions to a core of α-Zr(O). Thus, the specimens cannot be considered true equilibrium mixtures, and comparison of the results with phase diagram predictions is hazardous at best.

The upper pyrometer in Fig. 4 measured radiation emitted from a relatively thin layer of two-phase material at the specimen surface. The O/Zr gradient across this layer after annealing was probably fairly low, as indicated by the reasonably uniform distribution of phases in Fig. 3. Hence, the layer can be considered as being in pseudo-equilibrium, i.e., approximating to an equilibrium [α-Zr(O) + ZrO_{2-x}] mixture.

Fig. 9(a) shows a schematic section of the Zr-O phase diagram, illustrating two extreme cases of the possible reaction paths. Fig. 9(b) shows schematic PDTA traces that would be expected in each case. For this discussion, we assume that the 1773 K annealing period produced a

Table 1
Transition temperature values (K) from PDTA results

Ramp rate (K/min)	Heating Cycles							
	T_o			Mean T_o	T_{eo}			Mean T_{eo}
	1st cycle	2nd cycle	3rd cycle		1st cycle	2nd cycle	3rd cycle	
19 ± 0	1782	1781	1784	1782	1785	1785	1785	1785
28 ± 0	1781	1781	1778	1780	1783	1783	1782	1783
37 ± 0	1781	1780	1778	1780	1785	1782	1784	1784
86 ± 1	1783	1782	1784	1783	1786	1787	1787	1787
176 ± 2	1788	1788	1788	1788	1794	1792	1792	1793
318 ± 1	1792	1790	1789	1790	1797	1797	1797	1797
434 ± 2	1792	1791	1790	1791	1802	1802	1800	1801
569 ± 4	1791	1792	1789	1791	1802	1803	1803	1803
Ramp rate (K/min)	Cooling cycles							
	T_o			Mean T_o	T_{eo}			Mean T_{eo}
	1st cycle	2nd cycle	3rd cycle		1st cycle	2nd cycle	3rd cycle	
19 ± 0	1786	1785	1785	1785	1782	1784	1787	1784
28 ± 0	1787	1786	1782	1785	1783	1782	1782	1782
37 ± 0	1784	1784	1784	1784	1780	1780	1782	1781
70 ± 1	1784	1786	1785	1785	1779	1779	1779	1779
179 ± 1	1789	1789	1790	1789	1782	1782	17785	1783
332 ± 1	1790	1789	1790	1790	1783	1782	1783	1783
450 ± 2	1785	1785	1785	1785	1780	1780	1780	1780
509 ± 1	1785	1785	1785	1785	1779	1779	1779	1779

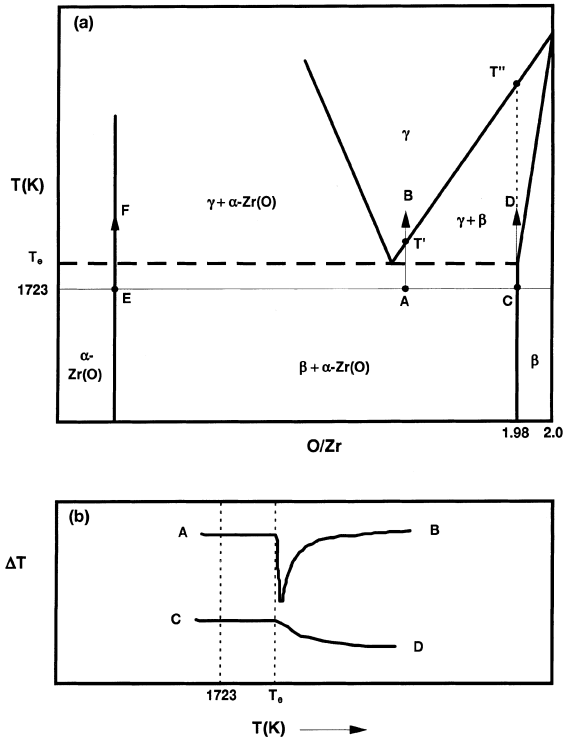

Fig. 9. Schematic diagrams illustrating: (a) possible reaction paths within the Zr–O phase diagram; and (b) corresponding PDTA traces.

two-phase surface composition close to the eutectoid composition (O/Zr ratio ~1.75), say, at point A.

Very slow heating, to allow time for oxygen transport, would move the system vertically towards B, with formation of γ-ZrO_{2-x} within the relatively short temperature interval between T_e and T'. The resulting PDTA trace would show a correspondingly sharp endothermic peak, with an onset temperature of T_e. This is illustrated by trace A → B in Fig. 9(b).

At very high heating rates, however, there would be insufficient time for oxygen transport to occur between the α-Zr(O) + β-ZrO_{2-x} phases, so that each phase would behave almost independently. Thus, the β-ZrO_{2-x} and α-Zr(O) phases would follow reaction paths C → D and E → F, respectively. The transition from β-ZrO_{2-x} to γ-ZrO_{2-x} would start at T_e, and would continue until T'' was reached. From Fig. 2, T'' is ~2300 K, i.e., well beyond the range of the PDTA measurements. Hence, the corresponding PDTA trace, illustrated as trace C → D in Fig. 9(b), would show a very shallow peak that failed to return to the baseline before heating had been terminated. In this case, the point of peak departure from the trace baseline would be hard to distinguish.

These two hypothetical cases represent extreme situations in the competition between O diffusion and specimen heating for the establishment of pseudo-equilibrium at the specimen surface. Hence, the fact that the observed PDTA peaks were relatively sharp and extremely reproducible between heating cycles would seem to imply that O transport, either within the ZrO_{2-x} and/or α-Zr(O) phases or along grain boundaries, was sufficiently rapid to outweigh the effect of rapid heating, thereby maintaining pseudo-equilibrium in the surface layer.

It is somewhat harder to explain why the onset temperatures for the exothermic peaks recorded during cooling were almost identical to those of the endothermic peaks recorded during heating. If the exothermic peak was produced by transformation of γ-ZrO_{2-x}–β-ZrO_{2-x}, the peak would be expected to *terminate* at T_e. Assuming pseudo-equilibrium at the specimen surface, the onset temperatures of the endothermic and exothermic peaks should only coincide if the annealing process had produced a mean O/Zr ratio in the surface layer equal to that of the eutectoid point in Fig. 2. This is not an unreasonable suggestion, however, given the relatively high concentration of α-Zr(O) that was observed within the surface layers.

4.2. Accuracy of the results

Both pyrometers used in this study had been factory calibrated using a black-body standard, with the calibration accuracy and repeatability quoted as ±1% (±16 K) and ±0.3% (±5 K), respectively, of the measurement range. The Fe melting-point results, however, suggest that the pyrometer calibration accuracy was considerably better than the quoted value of ±16 K.

The results in Table 1 indicate an increase of up to ~11 K in T_o values measured at higher heating rates. The T_o values measured during cooling, however, showed remarkably little variation with cooling rate. It seems reasonable to attribute the relatively small changes in T_o over such a wide range of heating/cooling rates to thermal lag effects. Thus, although T_o appears to be independent of heating/cooling rate, the thermal lag errors need to be included in the error estimate.

The following errors were considered: the Fe melting-point calibration error (±1 K), the pyrometer reproducibility (±5 K), the maximum thermal lag error (±11 K), the uncertainty in estimating peak-onset temperatures (±2 K) and errors introduced by rounding-off temperatures to the nearest degree (±1 K). An overall temperature uncertainty of ±12 K was derived from individual errors (ε) as $(\sum \varepsilon^2)^{1/2}$. Hence, based on the full set of PDTA results, the recommended value for T_e, the eutectoid-reaction-isotherm temperature, is 1786 ± 12 K. This result is in excellent agreement with the value of 1783 ± 7 K derived from the isothermal steam-oxidation data of Prater and Courtright [3].

5. Conclusions

A pyrometer based DTA method has been used to measure the temperature at which the $\beta/\beta + \gamma$ eutectoid transition occurs in ZrO_{2-x}. The transition appears to be completely reversible, shows no hysteresis, and is essentially insensitive to ramp rates within the ranges 19–569 K/min during heating or 19–509 K/min during cooling. Calibration of the method using the melting point of pure Fe confirmed the accuracy of temperature measurement as being considerably better than the pyrometer specifications of ±16°C. Based on the full data set, we recommend a value of 1786 ± 12 K for the eutectoid isotherm temperature.

The apparent insensitivity of the eutectoid transition temperature to heating rate is particularly relevant to cladding oxidation models that are based on the premise of using isothermal Zircaloy/steam reaction rates to predict oxidation rates during a high temperature transient. If this premise is correct, the present results indicate that the eutectoid-reaction temperature, above which there is a step increase in isothermal oxidation rate, can be considered as a constant in transient-oxidation models, regardless of the heating rate. The detailed transition mechanism remains unclear, however, especially with regard to its apparently complete reversibility at high heating/cooling rates. A tentative explanation has been proposed, based on the assumption of pseudo-equilibrium within the outer specimen layers. Nevertheless, the phenomenon is undoubtedly worthy of further study.

Acknowledgements

We thank D.B. Sanderson, A.J. White and D.G. Evans for useful manuscript reviews. We are particularly indebted to an anonymous referee for pointing out serious errors of interpretation in an earlier version of this report. Financial support from the CANDU Owners Group, consisting of AECL, Ontario Hydro, Hydro-Quebec and NB Power, is gratefully acknowledged.

References

[1] B.J. Hanna (Ed.), unpublished work, issued as AECL Report COG-93-140, RC-982-3.
[2] V.F. Urbanic, T.R. Heidrick, J. Nucl. Mater. 75 (1978) 251.
[3] J.T. Prater, E.L. Courtright, NUREG/CR-4889, PNL-6166, Pacific Northwest Laboratory, Richland, WA, 1987.
[4] A. Sawatzky, G.A. Ledoux, unpublished work, issued as AECL Report CANDEV-86-13.
[5] S. Leistikow, G. Schanz, Nucl. Eng. Design 103 (1987) 65.
[6] R.E. Pawel, J.V. Cathcart, R.A. McKee, J. Electrochem. Soc. 126 (1979) 1105.
[7] L. Baker, L.C. Just, ANL-6548, Argonne National Laboratory, Argonne, IL, 1962.
[8] E.G. Rauh, S.P. Garg, J. Am. Ceram. Soc. 63 (1980) 239.
[9] J.P. Abriata, J. Garces, R. Versaci, Bull. Alloy Phase Diagrams 7 (1986) 116.
[10] W.E. Wang, D.R. Olander, J. Amer. Ceram. Soc. 76 (1993) 1242.
[11] J.T. Prater, E.L. Courtright, in: Zirconium in the Nuclear Industry, seventh Symposium, ASTM-STP-939, 1987, p. 489.
[12] K.T. Conlon, C. Wong, J.W. DeVaal, B.H. McDonald, unpublished work, issued as AECL Report COG-91-270, RC-738.
[13] Anonymous, Point Lepreau Safety Report, Part 2, Revised 1994 May.
[14] A.R. West, Solid State Chemistry and its Applications, Wiley, New York, 1984.